where E is effective dose estimate and k=0.017 mSv× $mGy^{-1} \times cm^{-1}$. This value is applicable to chest scans and is the average between male and female models [19].

Calcium scoring

The Agatston [5], calcium volume [6] and mass [7] were determined on a commercially available external workstation (Advantage Windows Version 4.2, GE Healthcare, Waukesha, WI) and CAC-scoring software (Smartscore Version 3.5) according to the following equations:

1. *Agatston score = slice increment/ slice thickness* × ∑ (*area* × *cofactor*)
2. *Volume* = ∑ (*area* × *slice increment*)
3. *Mass* = ∑ (*area* × *slice increment* × *mean CT density*) ×*calibration factor* [20]

All CT scans were independently scored by two radiologists with 7- and 1-year experience of CAC measurement (observers 1 and 2, respectively). We performed biweekly CT scanner quality-control checks using an anthropomorphic phantom. A torso phantom for patient-based calibration was not used.

Statistical analyses

Each of the Agatston, volume and mass scores for the two observers were compared between image reconstructions

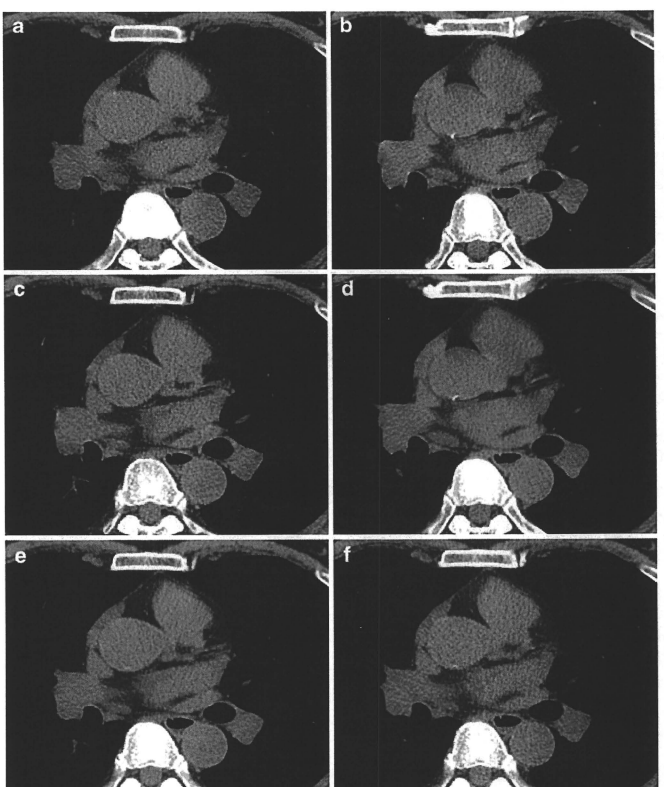

Fig. 1 A 45-year-old symptomatic man's transaxial images from first 1.25-mm-thickness prospective CT (**a**), second 1.25-mm-thickness prospective CT (**b**), first 2.5-mm-thickness prospective CT (**c**), second 2.5-mm-thickness prospective CT (**d**), first 2.5-mm-thickness retrospective CT (**e**) and second 2.5-mm-thickness retrospective CT (**f**) show heart. Calcium score for high density spot on left anterior descending artery was positive on images (**b**) and was negative on images (**a**), (**c**), (**d**), (**e**) and (**f**)

(1.25-mm prospective, 2.5-mm prospective and 2.5-mm-overlapping retrospective) and the two repeated scans (repeated measures ANOVA).

Next, for patients with positive CAC measurement on all scans, interscan variability between the two repeated scans was calculated by using the percentage difference in calcium scores.

The interscan variability
$= [absolute(scan1 - scan2)/(scan1 + scan2) \times 0.5] \times 100$

The interscan variability was compared between image reconstructions and scoring algorithms (two-factor factorial ANOVA). This was performed on CAC scores measured by the two observers.

Furthermore, interobserver variability was compared between image reconstructions and scoring algorithms, both on scan 1 and scan 2 (two-factor factorial ANOVA).

Lastly, mean and standard deviation (SD) of CT values, in regions of interest set in the aorta at the level of the left coronary artery, were measured by observer 1 and then the value mean + 2× SD and signal-to-noise ratio were calculated. These values were compared between three reconstruction images on scan 1 (one-factor ANOVA or Kruskal-Wallis, depending on the distribution of the data).

All statistical analyses were performed by using a commercially available software package (Statcel2, Saitama, Japan). For statistical analyses, repeated measures ANOVA (multivariate calculations), two-factor factorial ANOVA, one-factor ANOVA and Kruskal-Wallis were used to determine differences. When statistical significance was observed by ANOVA, the results were made post hoc by Scheffé test for multiple pairwise comparisons. P-values <0.05 were considered to identify significant differences.

Results

All patients were able to hold their breath on the four CT scans. Scan time was 10.0±1.9 s and 6.4±0.6 s on prospective and retrospective scans (scan 1), respectively. The DLPs were 89.0±8.5 mGycm, 89.0±8.5 mGycm, 266.4±23.1 mGycm and 265.3±22.6 mGycm on the first prospective, second prospective, first retrospective and second retrospective scans, respectively.

Seventy-six of the overall 100 patients had CAC deposits on all six CT reconstruction images and 33 patients had no CAC deposits on all six scans. There was one patient, showing positive CAC scores on the second 1.25-mm-thickness prospective scan, whereas negative CAC scores on the other five reconstruction images (Fig. 1). For patients with positive CAC measurements, the mean heart rate was 63±11 bpm (range, 44–101 bpm) on the first prospective scan (scan 1).

Table 1 Agatston, volume and mass scores on 1.25-mm prospective, 2.5-mm prospective and 2.5-mm/1.25-mm retrospective scans

	Agatston	Volume	Mass
1.25-mm prospective			
Reader 1			
Scan 1	589±910 (243)	469±699 (219)	120±185 (45)
Scan 2	581±877 (240)	463±673 (213)	120±183 (47)
Reader 2			
Scan 1	600±930 (242)	478±714 (207)	122±187 (45)
Scan 2	588±897 (235)	469±690 (197)	120±182 (46)
2.5-mm prospective			
Reader 1			
Scan 1	550±878 (197)	445±680 (172)	102±162 (37)
Scan 2	529±818 (212)	430±635 (181)	101±157 (41)
Reader 2			
Scan 1	552±902 (192)	447±700 (171)	103±165 (37)
Scan 2	531±832 (209)	433±651 (185)	101±158 (40)
2.5-mm/1.25-mm retrospective			
Reader 1			
Scan 1	496±748 (201)	403±577 (189)	93±143 (38)
Scan 2	597±772 (205)	403±594 (171)	94±146 (37)
Reader 2			
Scan 1	506±784 (200)	413±608 (176)	94±145 (38)
Scan 2	505±780 (213)	412±605 (180)	95±146 (38)

1.25-mm prospective: 1.25-mm thickness images on propective ECG-triggered scan
2.5-mm prospective: 2.5-mm thickness images on propective ECG-triggered scan
2.5-mm/1.25-mm retrospective: 2.5-mm thickness images with 1.25-mm increment on retrospective ECG-gated scan
Data are expressed as mean± standard deviation (median)

Coronary artery calcium scores

The Agatston, volume and mass scores for the two observers are summarized in Table 1. For observer 1, repeated measures ANOVA revealed that there was no statistical significance between repeated scans (Agatston; $p=0.17$, volume; $p=0.17$ and mass; $p=0.69$) and image reconstructions (Agatston; $p=0.81$, volume; $p=0.84$ and mass; $p=0.59$). For observer 2, also repeated measures ANOVA revealed no statistical significance between repeated scans (Agatston; $p=0.15$, volume; $p=0.16$ and mass; $p=0.23$) and image reconstructions (Agatston; $p=0.81$, volume; $p=0.85$ and mass; $p=0.60$).

Interscan variability

The interscan variability in Agatston, volume and mass scores on the three image reconstructions by two observers are shown in Fig. 2. For observer 1, two-factor factorial ANOVA revealed that there was no statistical significance between scoring algorithms ($p=0.13$); however, there were image reconstructions ($p<0.01$). The Scheffé test revealed statistical significance between the 1.25-mm prospective scan and 2.5-mm prospective scan ($p<0.01$) and between the 2.5-mm prospective scan and 2.5-mm retrospective scan ($p<0.01$). For observer 2, two-factor factorial ANOVA revealed that there was no statistical significance between scoring algorithms ($p=0.07$); however, there was image reconstructions ($p<0.01$). The Scheffé test revealed statistical significance between the 1.25-mm prospective scan and 2.5-mm prospective scan ($p<0.01$). Among image reconstructions, the 1.25-mm prospective scan showed the lowest variability. The 2.5-mm prospective scan on Agatston score showed high variability, that however on volume or mass scoring showed variability of around 10%, comparable to the 2.5-mm retrospective scan.

Interobserver variability

The interobserver variability in Agatston, volume and mass scores on the three image reconstructions in scan 1 and 2 are shown in Fig. 3. Two-factor factorial ANOVA revealed that there was no statistical significance between scoring algorithms (scan 1; $p=0.90$, scan 2; $p=0.43$) and image reconstructions (scan 1; $p=0.43$, scan 2; $p=0.79$). The interobserver variability was small. The mean percentage differences ranged from 5% to 14%, and the median 2% to 5%.

Image quality

The mean, SD, mean +2× SD and signal-to-noise ratio of CT values in regions of interest are summarized in Table 2. There was no significant difference in the mean value (one-factor ANOVA, $p=0.84$); however, there was in the SD (Kruskal-Wallis, $p<0.01$), mean +2× SD (one-factor ANOVA, $p<0.01$) and signal-to-noise ratio (Kruskal-Wallis, $p<0.01$).

Discussion

Among factors influencing interscan variability on CAC, the partial volume effect is known to be a major contributor. To reduce this, the use of thin-slice images [21, 22] or overlapping image reconstruction [12, 15, 23, 24] has been suggested. Two breath-holds [9] and change

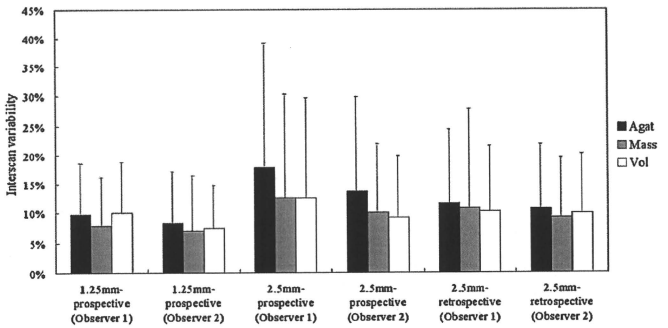

Fig. 2 The interscan variability of Agatston, volume and mass scores on 1.25-mm prospective, 2.5 mm prospective and 2.5-mm retrospective scans (two observers). Graph shows means (bars) and standard deviations (vertical lines). For observer 1, two-factor factorial ANOVA revealed that there was not significant difference of interscan variability between scoring algorithms ($p=0.13$); however, there was between image reconstructions ($p<0.01$). For observer 2, also two-factor factorial ANOVA revealed that there were not significant differences between scoring algorithms ($p=0.07$); however, there were between image reconstructions ($p<0.01$)

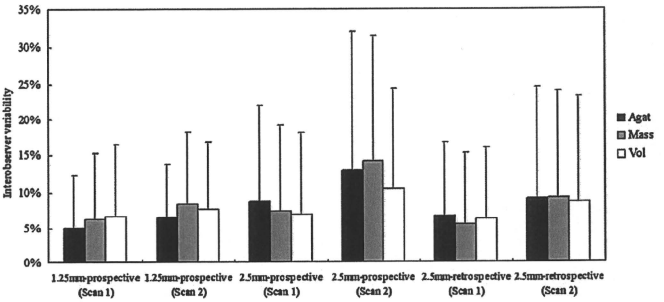

Fig. 3 The interobserver variability of Agatston, volume and mass scores on 1.25-mm prospective, 2.5-mm prospective and 2.5-mm retrospective scans (scan 1 and 2). Graph shows means (bars) and standard deviations (vertical lines). Two-factor factorial ANOVA revealed that there was no statistical significance between scoring algorithms (scan 1; p=0.90, scan 2; p=0.43) and image reconstructions (scan 1; p=0.43, scan 2; p=0.79)

of heart rate [25] in the examination are also known factors responsible for reducing reproducibility of CAC measurement. A long scanning time in thin-slice prospective ECG-triggered CT had discouraged its use up until the era of 4-slice CT. Thin-slice prospective ECG-triggered scan in a breath-hold has been possible with the advent of 16- or 64-slice CT, thus motivating us to perform this study.

Interscan variability

Multi-slice CT with retrospective ECG-gated spiral overlapping images has been shown to have low interscan variability of CAC measurement [12, 15]. As expected, 1.25-mm-thickness prospective ECG-triggered scan showed the lowest variability in repeated measurement of CAC by virtue of the reduced partial volume effect. The results were satisfactory in all scoring algorithms. Unexpectedly, the results of 2.5-mm-thickness prospective ECG-triggered scan with volume and mass scoring algorithms were also satisfactory. The reasons are not clear; however, some ideas to explain this have been put forward. They include scan start delay (4 to 5 s after holding the breath), high image quality and short scanning time. The scanning time of prospective ECG-triggered scan in the current study was around 10 s, however still longer than that of the retrospective ECG-gated spiral scan. This is because we used a configuration of 1.25-mm collimation width ×16 detectors on prospective ECG-triggered scan, to reconstruct both 1.25-mm- and 2.5-mm-thickeness images. Reproducibility of CAC measurement on 2.5-mm-thickness prospective ECG-triggered scans might further improve if a configuration of 2.5-mm collimation ×16 detectors is used, as change of heart rate in the examination would decrease.

Interobserver variability

Interobserver variation is an important source of differences in CAC measurement. In electron-beam CT, intra-observer and interobserver reliability for CAC has been shown to be small. Apart from the second 2.5-mm prospective scan (scan 2), our results were mostly comparable to those on retrospective ECG-gated single-slice spiral CT [26], although half of the CAC measurements were performed by a less-experienced radiologist (1 year).

Table 2 Mean and standard deviation of CT values in regions of interest set in the aorta at the level of the left coronary artery (scan 1 measured by observer 1, n=100)

	Mean	SD	Mean +2×SD	Signal-to-noise ratio
1.25-mm prospective	40	20	81 (ranged 45–106)	2.06
2.5-mm prospective	40	15	69 (ranged 45–105)	2.86
2.5 mm/1.25 mm retrospective	40	22	83 (ranged 55–114)	1.93
Statistics	ns (p=0.84)	s (p<0.01)	s (p<0.01)	s (p<0.01)
	ANOVA	Kruskal-Wallis	ANOVA	Kruskal-Wallis

SD: standard deviation
Signal-to-noise ratio=mean/standard deviation
s: significant, ns: not significant
ANOVA: one-factor ANOVA

Coronary artery calcium measurement using thin-slice images

When applying 1.25-mm-thickness images for CAC scoring, noise is a problematic issue. In some literature, to exclude a false-positive depiction of image noise as calcification in thin-slice CT study, the detection threshold for CAC was elevated from 130 HU to 350 HU [27, 28]. We consider, however, that this method entails a significant disadvantage: decreased sensitivity for detection of small CAC plaque, i.e., leading to false-negative measurements. This problem, regretfully, cannot be overcome unless the radiation dose is increased.

Another concern is the difference of CAC scores between 1.25-mm and 2.5-mm slice thicknesses, caused by the partial volume effect. Some studies show that thinner slices lead to significantly increased CAC results [23, 27], although one study shows no significant difference [29]. The current study showed that the three CAC scores on 1.25-mm prospective ECG-triggered tended to be higher than both those on 2.5-mm prospective ECG-triggered and 2.5-mm retrospective ECG-gated scans. Vliegenthart et al. [22], on electron beam CT study, have suggested that partial volume effects on 3.0-mm images may lead to underestimation or even complete disregard of small or low-density calcifications. In a study using a cardiac phantom, also thin-slice images are shown to have an impact on the measurement accuracy of CAC volume [30].

Thus, as mentioned above, thin-slice images have advantages in reproducibility of CAC measurement, detectability of subtle CAC plaque and measurement accuracy of CAC. The drawback is requiring a high radiation dose to maintain the image quality needed. Mühlenbruch et al. showing similar calcium scoring results of 1-mm and 3-mm slices, conclude that 'the potentially necessary increase of the patient's dose in order to achieve assessable 1-mm slices with an acceptable image-to-noise ratio appears not to be justified' [31].

Effect of volume and mass scoring algorithms

Neither volume nor mass algorithm had an impact on reducing the variability on 1.25-mm prospective ECG-triggered and 2.5-mm spiral retrospective ECG-gated scans. Similar results were observed in the study using 2.5-mm spiral retrospective ECG-gated scans on 16-slice CT [15]. We believe this is due to the potential reduction of partial volume effect in these protocols. Although the Agatston method intrinsically has the step function [7] increasing the variability, other factors such as motion artifacts and image quality were considered to be the dominant. In contrast to this, volume and mass algorithms were effective in reducing the variability on 2.5-mm prospective ECG-triggered scan.

Limitation

The limitation of the study is radiation dose, which is a critical issue for a CAC measurement protocol being accepted as a screening or a follow-up modality. The effective radiation dose of 1.5 mSv on prospective scans in the current study is higher than those of electron beam CT (1.0 mSv for men and 1.3 mSv for women) [32]. Noise level (standard deviation of CT value) should be controlled within a reasonable level, such as 20 HU [11]. The value (CT value +2× SDs) should be less than the CAC detecting threshold of 130 HU [33]. Keeping these levels, radiation dose should be reduced to as low as achievably possible for individuals based on body weight or body mass index.

In conclusion, prospective electrocardiograph-triggered 64-slice CT using the 1.25-mm prospective scan shows the lowest variability. The 2.5-mm prospective scan on volume or mass scoring shows variability of around 10%, comparable to 2.5-mm-thickness spiral overlapping reconstruction images. For reduction of radiation exposure and monitoring of CAC over time and over CT scanners, 2.5-mm-thickness images using a mass algorithm is considered recommendable.

References

1. Callister TQ, Raggi P, Cooil B, Lippolis NJ, Russo DJ (1998) Effect of HMG-CoA reductase inhibitors on coronary artery disease as assessed by electron-beam computed tomography. N Engl J Med 339:1972–1978
2. Maher JE, Bielak LF, Raz JA, Sheedy PF II, Schwartz RS, Peyser PA (1999) Progression of coronary artery calcification: a pilot study. Mayo Clin Proc 74:347–355
3. Janowitz WR, Agatston AS, Viamonte M Jr (1991) Comparison of serial quantitative evaluation of calcified coronary artery plaque by ultrafast computed tomography in persons with and without obstructive coronary artery disease. Am J Cardiol 68:1–6
4. Fischbach R, Heindel W (2000) Detection and quantification of coronary calcification: an update. Rofo 172:407–414
5. Agatston AS, Janowitz WR, Hildner FJ, Zusmer NR, Viamonte M, Detrano R (1990) Quantification of coronary calcium using ultrafast computed tomography. J Am Coll Cardiol 15:827–832
6. Callister TQ, Cooil B, Raya SP et al (1998) Coronary artery disease: improved reproducibility of calcium scoring with an electron-beam CT volumetric method. Radiology 208:807–814

7. Yoon HC, Greaser III LE, Mather R, Sinha S, McNitt-Gray MF, Goldin JG (1997) Coronary artery calcium: alternate methods for accurate and reproducible quantitation. Acad Radiol 4:666–673
8. Wang SJ, Detrano BC, Secci A et al (1996) Detection of coronary calcification with electron-beam computed tomography: evaluation of interexamination reproducibility and comparison of three image-acquisition protocols. Am Heart J 132:550–558
9. Achenbach S, Ropers D, Mohlenkamp S et al (2001) Variability of repeated coronary artery calcium measurements by electron beam tomography. Am J Cardiology 87:210–213
10. O'Rourke RA, Brundage BH, Froelicher VF et al (2000) American College of Cardiology/American heart association expert consensus document on electron-beam computed tomography for the diagnosis and prognosis of coronary artery disease. Circulation 102:126–134
11. McCollough CH, Ulzheimer S, Halliburton SS, White RD, Kalender WA (2003) A multi-scanner, multi-manufacture, international standard for the quantification of CAC using cardiac CT (abstr). In: Radiological society of North America scientific assembly and annual meeting program. Radiological Society of North America, Oak Brook, Ill 630–631
12. Ohnesorge B, Flohr T, Fischbach R et al (2002) Reproducibility of coronary calcium quantification in repeat examinations with retrospectively ECG-gated multisection spiral CT. Eur Radiol 12:1532–1540
13. Van Hoe LR, De Meerleer KG, Leyman PP, Vanhoenacker PK (2003) Coronary artery calcium scoring using ECG-gated multidetector CT: effect of individually optimized image-reconstruction windows on image quality and measurement reproducibility. AJR 181:1093–1100
14. Daniell AL, Wong ND, Friedman JD et al (2003) Reproducibility of coronary calcium measurements from multidetector computed tomography. J Am Coll Cardiol 41:456A
15. Horiguchi J, Yamamoto H, Akiyama Y et al (2005) Variability of repeated coronary artery calcium measurements by 16-MDCT with retrospective reconstruction. AJR 184:1917–1923
16. Ulzheimer S, Kalender WA (2003) Assessment of calcium scoring performance in cardiac computed tomography. Eur Radiol 13:484–497
17. Horiguchi J, Fukuda H, Yamamoto H et al (2007) The impact of motion artifacts on the reproducibility of repeated coronary artery calcium measurements. Eur Radiol 17:81–86
18. Horiguchi J, Shen Y, Hirai N et al (2006) Timing on 16-slice scanner and implications for 64-slice cardiac CT: Do you start scanning immediately after breath-hold? Acad Radiol 13:173–176
19. Morin RL, Gerber TC, McCollough CH (2003) Radiation dose in computed tomography of the heart. Circulation 107:917–922
20. Hong C, Bae KT, Pilgram TK, Suh J, Bradley D (2002) Coronary artery calcium measurement with multi-detector row CT: in vitro assessment of effect of radiation dose. Radiology 225:901–906
21. Callister T, Janowitz W, Raggi P (2000) Sensitivity of two electron beam tomography protocols for the detection and quantification of coronary artery calcium. AJR 175:1743–1746
22. Vliegenthart R, Song B, Hofman A, Witteman JCM, Oudkerk M (2003) Coronary calcification at electron-beam CT: Effect of section thickness on calcium scoring in vitro and in vivo. Radiology 229:520–525
23. Achenbach S, Meissner F, Ropers D et al (2001) Overlapping cross-sections significantly improve the reproducibility of coronary calcium measurements by electron beam tomography: a phantom study. JCAT 25:569–573
24. Kopp AF, Ohnesorge B, Becker C et al (2002) Reproducibility and accuracy of coronary calcium measurements with multi-detector row versus electron-beam CT. Radiology 225:113–119
25. Mao S, Budoff MJ, Bakhsheshi H, Liu SCK (2001) Improved reproducibility of coronary artery calcium scoring by electron beam tomography with a new electrocardiographic trigger method. Invest Radiol 36:363–367
26. Goldin JG, Yoon HC, Greaser III LE et al (2001) Spiral versus electron-beam CT for coronary artery calcium scoring. Radiology 221:213–221
27. Muhlenbruch G, Thomas G, Wildberger JE et al (2005) Effect of varying slice thickness on coronary calcium scoring with multislice computed tomography in vitro and in vivo. Invest Radiol 40:695–699
28. Hong C, Becker CR, Schoepf UJ et al (2002) Coronary artery calcium: absolute quantification in nonenhanced and contrast-enhanced multidetector row CT studies. Radiology 223:474–480
29. Mao S, Child J, Carson S et al (2003) Sensitivity to detect small coronary artery calcium lesions with varying slice thickness using electron beam tomography. Invest Radiol 38:183–187
30. Horiguchi J, Shen Y, Akiyama Y et al (2006) Electron beam CT versus 16-slice spiral CT: how accurately can we measure coronary artery calcium volume? Eur Radiol 16:374–380
31. Mühlenbruch G, Klotz E, Wildberger JE et al (2007) The accuracy of 1- and 3-mm slices in coronary calcium scoring using multi-slice CT in vitro and in vivo. Eur Radiol 17:321–329
32. Hunold P, Vogt FM, Schmermund A et al (2003) Radiation exposure during cardiac CT: Effective doses at multi-detector CT and electron-beam CT. Radiology 226:145–152
33. Bielak LF, Kaufmann RB, Moll PP, MacCollough CH, Schwartz RS, Sheedy PF II (1994) Small lesions in the heart identified at electron beam CT: calcification or noise? Radiology 192:631–636

Circ J 2009; **73:** 691–698

Diagnostic Accuracy of Angiographic View Image for the Detection of Coronary Artery Stenoses by 64-Detector Row CT

—— A Pilot Study Comparison With Conventional Post-Processing Methods and Axial Images Alone ——

Masahiro Jinzaki, MD; Kozo Sato, MD; Yutaka Tanami, MD; Minoru Yamada, MS*; Toshihisa Anzai, MD**; Akio Kawamura, MD**; Koji Ueno, MD**; Sachio Kuribayashi, MD

Background: The angiographic view (AGV) image is a new post-processing method that is similar to conventional coronary angiography (CAG). The purpose of this study was to evaluate its accuracy for coronary stenosis detection by 64-detector row computed tomography (CT).

Methods and Results: CT evaluation results of 17 patients were compared with the results of invasive CAG on a coronary segment basis concerning the presence of stenoses >50% diameter reduction. All images of the 3 viewing methods (combination of conventional methods, AGV image alone, and axial images alone) were evaluated in consensus by 3 cardiovascular radiologists. Among 196 assessable segments, invasive CAG showed significant coronary artery stenoses in 44 segments. 43 of 44 lesions were detected with the AGV image, and absence of significant stenosis was correctly identified in 135 of 152 segments (sensitivity 98%; specificity 89%; accuracy 91%; positive predictive value 72%, negative predictive value 99%). The sensitivity of the AGV image was the same as that of conventional methods (98%). There was no significant difference in accuracy between the AGV image (91%) and conventional methods (94%). The accuracy of the AGV image was significantly higher than the axial images alone (78%).

Conclusions: AGV image shows promise as a post-processing method for identifying coronary artery stenosis with high accuracy. (*Circ J* 2009; **73:** 691–698)

Key Words: Computed tomography; Coronary angiography; Coronary artery disease; Maximum-intensity projection; Post-processing

Recent advances in multidetector-row computed tomography (MDCT) have enabled non-invasive evaluation of coronary artery stenoses with high accuracy.[1–4] Diagnostic evaluation of coronary artery stenoses includes review of the originally reconstructed axial images, as well as various post-processing images. The important role of post-processing images is to integrate the series of axial CT sections into a form that is easier to interpret and the axial images can be made to appear similar to other, more familiar images such as those from invasive angiography.[5–9] In these aspects, current methods, such as volume rendering (VR), partial maximum intensity projection (partial MIP), curved multiplanar reconstruction (curved MPR), or cross-sectional images, fall short. VR enables overview of the coronary artery to third parties, but it is not usually used for the evaluation of coronary artery stenoses. For coronary artery stenoses, partial MIP, curved MPR or cross-sectional images are used, but these conventional methods are quite different from the images obtained with invasive coronary angiography (CAG), and it can be difficult for a third person to understand which artery or segment is being analyzed.

The angiographic view (AGV) image is a MIP image in which contrast media in the ventricles is eliminated. This image is similar to that from invasive CAG and thus familiar to cardiologists. This type of MIP image clearly demonstrates the distribution of high-density lesions, such as coronary calcifications and stents, in the 1 image. If coronary artery stenoses can also be identified on the AGV image with high accuracy, it will be the post-processing method with most promise for accurately showing the distribution of coronary lesions that is understandable by third parties such as referral physicians and the patients.

In this study, we evaluated the accuracy of the AGV image in comparison with axial images alone and a combination of conventional methods for coronary stenoses detection.

(Received August 18, 2008; revised manuscript received November 21, 2008; accepted December 7, 2008; released online February 18, 2009)
*Department of Diagnostic Radiology, *Division of Cardiovascular Imaging Laboratory, Research Park and **Division of Cardiology, Department of Medicine, Keio University School of Medicine, Tokyo, Japan*

Mailing address: Masahiro Jinzaki, MD, Department of Diagnostic Radiology, Keio University School of Medicine, 35 Shinanomachi, Shinjuku-ku, Tokyo 160-8582, Japan. E-mail: jinzaki@sc.itc.keio.ac.jp

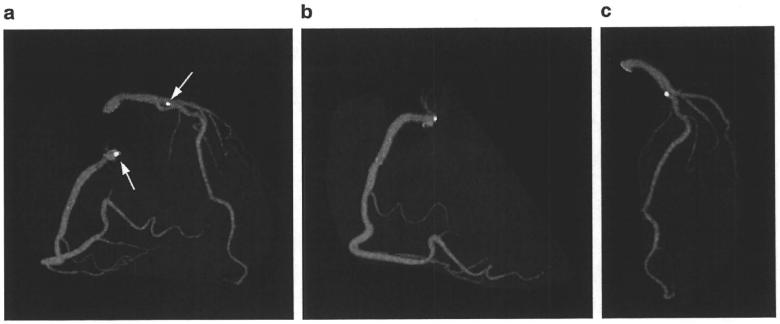

Figure 1. Angiographic view (AGV) of the coronary arteries (**a**) enables an overview of the coronary tree. The AGV is divided into right (**b**) and left (**c**) coronary artery, and viewed from various angles. The distribution of calcifications (arrows) is shown.

Table 1. Diagnostic Accuracy of Each Viewing Method: Test Characteristics by Segments

	Sensitivity	Specificity	PPV n/total n (%)	NPV	Accuracy
Angiographic view image	43/44 (98)	135/152 (89)	43/60 (72)	135/136 (99)	178/196 (91)
Conventional methods	43/44 (98)	141/152 (93)	43/54 (80)	141/142 (99)	184/196 (94)
Axial images alone	38/44 (86)	115/152 (76)	38/75 (51)	115/121 (95)	153/196 (78*)

*P<0.05 for angiographic view vs axial images alone and conventional methods vs axial images alone.
PPV, positive predictive value; NPV, negative predictive value.

Methods

Patient databases from the Catheter Angiography Laboratory and Radiology Department were reviewed for patients who had undergone both invasive CAG and CT CAG within 1 month and without other interventions in the meantime. We identified 18 consecutive patients from May 2005 to September 2005, but 1 was excluded because of atrial fibrillation. Thus, data of 17 patients (15 men, 2 women; 35–80 years, average 58 years) were available. The average heart rate (HR) of these patients was 58.6±6.6 beats/min (44–72 beats/min; 16 patients with HR<70 beats/min, 1 patient with HR>70 beats/min). Retrospective evaluation of patient data acquired during clinical routines is approved by the Institutional Review Board, and written informed consent was not obtained from the patients.

MDCT Data Acquisition

Computed tomography (CT) CAG was performed using 64-detector row CT (LightSpeed VCT: GE Healthcare, Milwaukee, WI, USA). Nitroglycerin spray (0.3 mg, glycerol trinitrate) was administered sublingually immediately before the scan;β -blocker was not administered prior to the scan. The delay between the start of injection and scanning was determined by the test bolus technique, monitoring at the level of the ascending aorta. The dynamic monitoring scans started 10 s after beginning the injection of intravenous contrast material (10 ml of contrast material followed by 15 ml of saline injected at 4 ml/s), and were obtained every 2 s with low-dose (120 kV, 20 mA).The delay applied for the main scanning was calculated by the time to peak enhancement for the test bolus plus 2 s. The main scanning was performed with 64×0.625 mm collimation, acquiring the entire heart within 5 to 6s. The gantry rotation time was 0.35s, and the pitch was between 0.20 and 0.22. The tube current was 350–550 mA at 120 kV. Iodine contrast material (40–60 ml; Iopamidol 370 mgI/ml) was immediately followed by 20 ml of saline, injected at a rate of 4 ml/s. The estimated effective radiation dose was 15–19 mSv. ECG-gated datasets were reconstructed automatically at 75% of the R-R interval and 45% of the R-R interval to create a stack of contiguous axial images with a section thickness of 0.625 mm and an increment of 0.625 mm. Depending on the HR, 2 reconstruction algorithms were applied: a single-segmental reconstruction (<70 beats/min) and multisector (2 or 4) reconstruction (>70 beats/min). If motion artifacts were present in any coronary artery, image reconstruction was repeated with the reconstruction window offset by 5% toward the beginning or end of the cardiac cycle, and multiple reconstructions were obtained until all arteries were depicted free of motion artifact or until reconstructions in 5% intervals throughout the cardiac cycle had been obtained.

Invasive CAG

Invasive CAG was performed by experienced cardiologists using standard techniques and the acquisition of standard projection planes. Stenosis severity was determined by quantitative CAG (QCA) (QuantCor.QCA,Pie Medical Imaging, Maastricht, The Netherlands). The grade of diameter stenosis (maximum diameter reduction) was determined by dividing the minimal diameter in the diseased segment by the diameter in the adjacent proximal disease-free section.

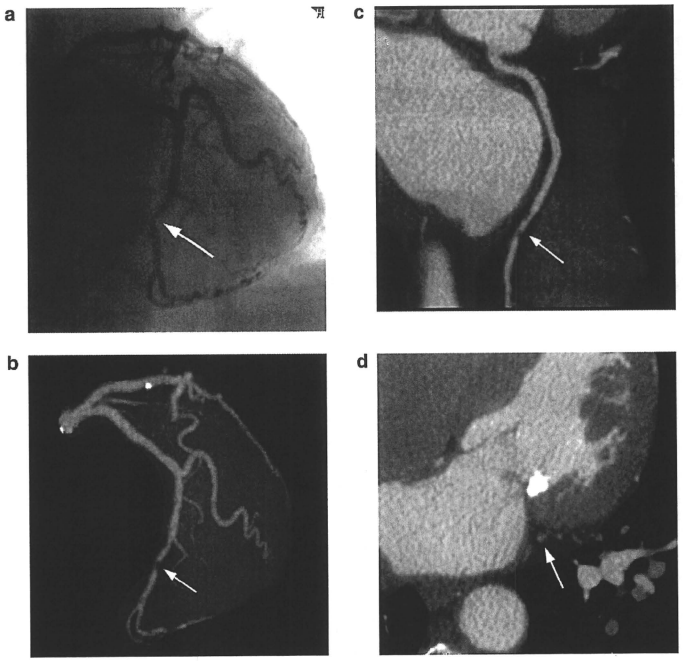

Figure 2. A 67-year-old woman with a significant stenosis in the distal left circumflex artery on the invasive angiogram (**a**: arrow). This lesion was correctly diagnosed as >50% stenoses with all viewing methods: angiographic view image (**b**: arrow), conventional methods (**c**: arrow), and axial images (**d**: arrow).

MDCT Image Analysis

CT axial images were transferred to a standard commercial workstation (GE Advantage Workstation 4.3) where the AGV image was automatically created as follows.

(1) The whole heart is extracted from the 3D volume data, after cutting and removing unnecessary regions such as bone, aorta and liver.

(2) Contrast medium within the endocardium is identified as ventricular.

(3) The ventricular area is subtracted from the whole heart image.

(4) MIP display of the image shows the coronary artery network identical to that seen with invasive CAG.

The AGV image can be spun around and viewed in various angles. Similar images can be created by tracking and extracting the coronary artery itself. However, tracking or extracting requires the threshold of CT attenuation, so the images can vary depending on the threshold, and the ability of the workstation used. The AGV image keeps the coronary artery untouched, and thus the image does not vary among workstations.

One technologist (4 years experience in cardiac CT imaging) who was unaware of the results of conventional CAG rendered curved MPR and AGV images. Curved MPRs were rendered with 0.6-mm section thickness, displaying all 15 segments of the AHA model in 2 orientations (with longitudinal and cross-sectional images as reference). Whether each coronary segment seen on the axial images was also identified by the conventional methods and on the AGV image was checked by this blinded technologist. The data sets were then stored for further analysis.

All images for the 3 viewing methods (ie, combination of conventional methods [axial images, partial MIP, partial MPR, and curved MPR], AGV image alone, and axial images alone) were evaluated in consensus by 3 cardiovascular radiologists: 2 with 5 years experience and 1 with 4 years experience in CT CAG. The readers were unaware of the patient's history, clinical details and QCA findings. First, the conventional methods were assessed, then the AGV image alone, and lastly the axial images alone, all at 2-week intervals. In the reading of the conventional methods, the readers interactively rendered partial MPRs or partial MIPs by using a 0.6-mm-thickness, and comprehensively reviewed these images, the axial images, and curved MPRs on the workstation. Axial images and curved MPRs were initially displayed with a default window setting (level, 100HU; window, 700HU). The AGV image was divided into the right and left coronary artery, similar to images from invasive CAG, and the readers viewed various angles of the images (**Figure 1**). The AGV image was initially dis-

Table 2. Location of False-Negative Lesions of Each Viewing Method

	Vessel branching out from mid-portion of the stent	Lesion located in the just proximal portion of the branch	Lesion located at the segment running horizontal to the axial section	Total
Angiographic view image	1	0	0	1
Conventional methods	0	1	0	1
Axial images alone	1	0	5	6

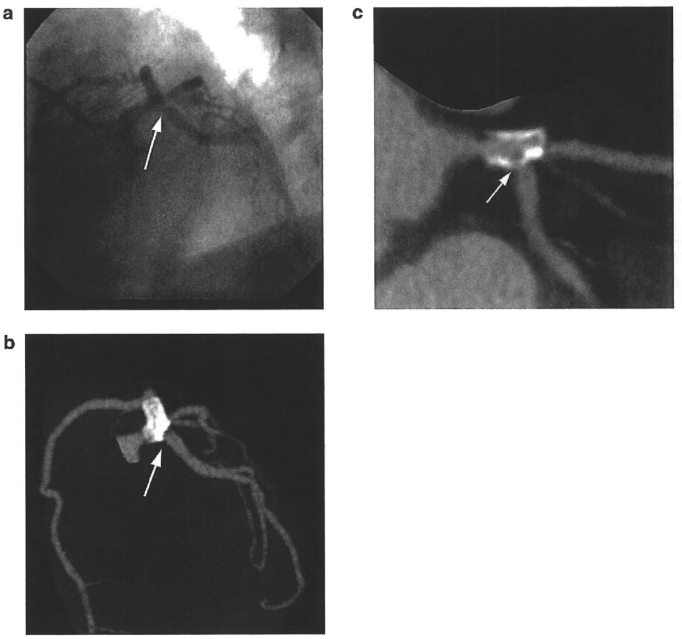

Figure 3. A 55-year-old man with a significant stenosis in the just proximal portion of the left circumflex artery on the invasive angiogram (**a**: arrow). This lesion was not detected (false negative) on the angiographic view image (**b**: arrow), but was correctly diagnosed as >50% stenosis by the conventional methods (**c**: arrow) and on the axial images (not shown).

played with a default window setting (level, 350 HU; window, 700 HU). The window and level of the evaluated images was then adjusted by the observer. Segments with severe calcifications (occupying more than half the circumference), stents, a vessel caliber less than 1.5 mm as defined on conventional CAG, or with a discontinuous area because of premature beat were excluded from the analysis.

All analyses were performed on a coronary segment basis (15 segments of the AHA model). Each segment was categorized by the presence or absence of a stenoses of 50% diameter reduction or more. MDCT evaluation results were documented in writing and then compared with the results of QCA. True positives were defined as correct identification by MDCT of segments of more than 50% diameter and true negatives were defined as correct identification by MDCT of segments of 50% or less. Segments that had inconsistencies between QCA and each viewing method were retrospectively re-evaluated by the 3 radiologists.

Statistical Analysis

The sensitivity, specificity, positive predictive value (PPV), and negative predictive value (NPV) of each of the viewing methods for detection of hemodynamically significant stenoses (≥50%) as compared with the reference standard (QCA) were calculated for each segment. We compared the accuracy of the different viewing methods for the detection of stenoses using McNemar's test. Statistical significance was considered to be present at $P<0.05$. Statistical analysis was performed using SPSS (version 13.0; SPSS, Chicago, IL, USA).

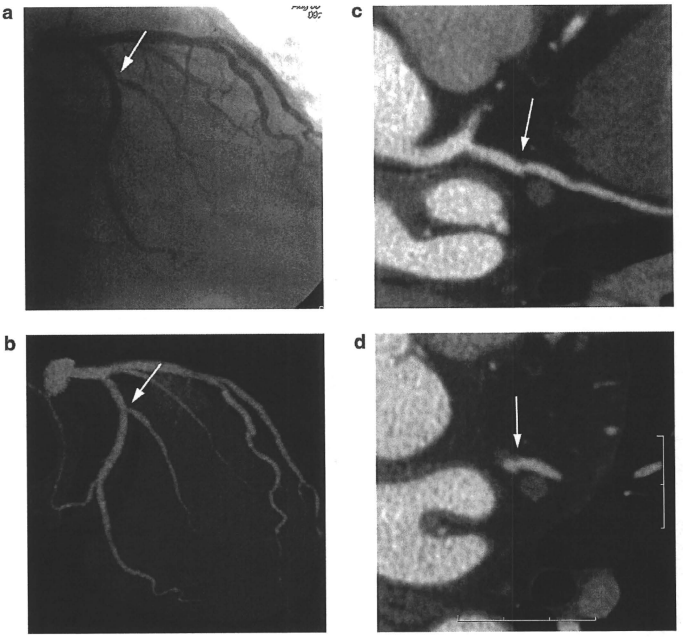

Figure 4. A 63-year-old man with a significant stenosis located in the just proximal portion of the obtuse marginal branch on the invasive angiogram (**a**: arrow). This lesion was diagnosed as >50% stenosis on the angiographic view image (**b**: arrow), but was judged to be <50% stenoses (false negative) with the conventional methods (**c**: arrow) and on the axial images (**d**: arrow).

Table 3. Results of Quantitative Coronary Angiography for False-Positive Lesions of Each Viewing Method

	Lesions with no severe calcification			Lesions with severe calcification			Total
	Mild stenosis	Trivial stenosis	No stenosis	Mild stenosis	Trivial stenosis	No stenosis	
Angiographic view image	7	1	1†	5	3	0	17
Conventional methods	3	1	0	4	3	0	11
Axial images alone	25	1	4	4	3	0	37

Mild stenosis: 26–50%; trivial stenosis: 1–25% stenoses.
†Muscular bridge.

Results

Of 208 segments >1.5 mm in diameter, 196 segments were included. Among the 12 segments excluded, 10 had stents and 2 were segments with a discontinuous area because of premature beat. QCA showed significant coronary artery stenoses (ie, 1 or more stenoses >50%) in 22% (44/196) of the segments. All coronary segments >1.5 mm in diameter and seen on the axial images were also identified by the conventional methods and on the AGV image.

Diagnostic Accuracy of Each Viewing Method

Table 1 shows the results of the 3 viewing methods for lesion detection by coronary artery segment. In the comparison of the AGV image and conventional methods, sensitivity was the same (98%) and there was no significant difference in accuracy (P>0.05: 91% with AGV image and 94% with conventional methods) (**Figure 2**). The accuracy of the AGV image was significantly higher compared with axial images alone (P<0.05).

False-Negative (FN) Lesions of Each Viewing Method

The location of the FN lesion differed among the viewing methods (**Table 2**).

With the AGV image, a FN lesion was located just proximal portion to the left circumflex artery where the vessel

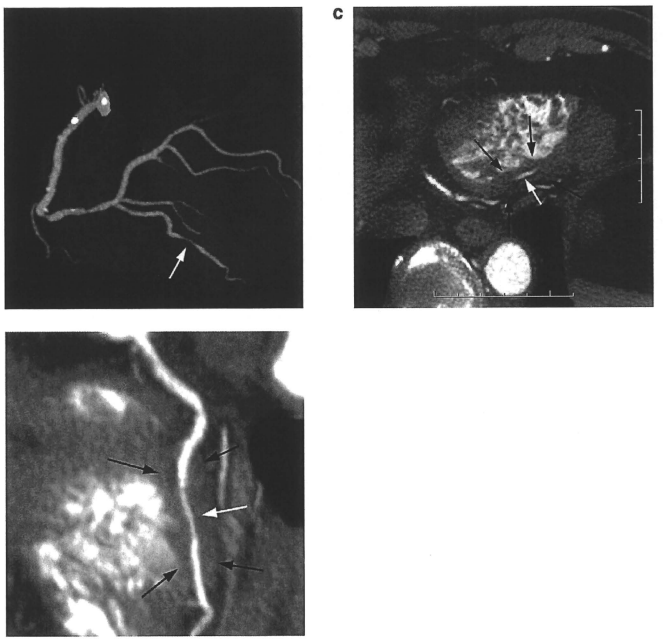

Figure 5. A 73-year-old man with a myocardial bridge in the poster descending branch. The lesion was judged as >50% stenosis on the angiographic view (**a**: arrow). With the conventional methods (**b**) and on the axial images (**c**), this lesion (white arrow) seemed to be >50% stenosis, but was judged to be a myocardial bridge not a stenotic lesion because of plaque, because myocardium (black arrows) was seen surrounding the lesion.

branched out from the mid-portion of the stent (**Figure 3**). This may have been a stent artifact, which appears to "bloom" the outer margin of the stent, hiding lesions in the just proximal portion from view.

With the conventional methods, a FN lesion was located in the just proximal portion of the obtuse marginal artery (**Figure 4**). This type of lesion can appear stenotic using projection methods such as the AG view and QCA, but as seen with the conventional methods, it may in fact be non-stenotic. However, if QCA is used as the gold standard, the result will be an AGV image true-positive and conventional false-negative.

With the axial images alone, 5 of 6 FN lesions were located in the segment running horizontal to the axial section, and the remaining 1 was the same as the FN lesion in the AGV image.

False-Positive (FP) Lesions of Each Viewing Method

The FP lesions for each viewing method varied with the results of QCA (**Table 3**). The FP lesions were divided into 2 categories: with and without severe calcification.

Lesions With Severe Calcification The total number of lesions with severe calcification was 24. On the AGV image, 5 of the 8 FP lesions with severe calcification were mild stenoses (26–50%), and 3 were trivial (1–25%). With the conventional methods and on the axial images alone, 4 of 7 FP lesions were mild stenoses and 3 were trivial stenoses. The "blooming" artifact of calcification was considered to cause the overestimation of mild or trivial stenoses. One severe calcification of a mild stenosis was FP only on the AGV image, and true-positive with the conventional methods and the axial images alone.

Lesions With No Severe Calcification The total number of lesions with no severe calcification was 172. On the AGV image, 7 of the 9 FP lesions with no severe calcification were mild stenoses, 1 was a trivial stenosis, and the other was a non-stenosis on QCA. Thus, the main cause of FP lesions on the AGV image was overestimation of mild stenoses as >50% stenoses. One trivial-stenotic lesion was accompanied by protruding moderate calcification (occupying less than 50% diameter), thus the blooming artifact of calcification was considered to cause the overestimation of trivial stenoses as >50% stenoses on the AGV image. One non-stenotic lesion on QCA was a myocardial bridge (**Figure 5**). This lesion was also viewed as stenotic by the conventional methods and on the axial images alone. However, those methods demonstrated the myocardium surrounding the vessel, and thus enabled the correct diagnosis of myocardial bridge not stenotic lesion because of plaque.

With the conventional methods, 3 of the 4 FP lesions were mild stenoses on QCA, and the other was a trivial stenosis (same as with the FP lesion on the AGV image ; the lesion was accompanied by protruding moderate calcification).

On the axial images alone, 25 of the 30 FP lesions were mild stenoses, 1 was a trivial stenosis, and 4 were non-stenoses on QCA. The number (n=30) of FP was much more than on the AGV images (n=9) or with the conventional methods (n=4). This was retrospectively considered to be related to evaluation of lesions located in the segment running horizontal to the axial section, and that diffuse concentric plaque with positive remodeling in all length of segment is more difficult to determine on axial images compared with other methods. Among the 30 FP lesions on the axial images alone, 14 were located in the segment running horizontal to the axial section (horizontal lesion), and 4 were diffuse concentric plaque with positive remodeling in all length of segment (concentric lesion). Among the 9 FP lesions on the AGV images, only 1 was a horizontal lesion and 0 with the conventional methods, and no concentric lesions with either method.

Discussion

The axial image is the basic clinical reference for detailed image analysis. However, because of the complex course of the coronary artery, interpretation of axial images may be difficult and the use of post-processing techniques enables investigators to better understand the complex coronary artery anatomy and abnormalities. There have been several studies of the use of various post-processing methods for CT CAG and according to their results, a combination of various viewing methods gives the highest sensitivity, and was used in most of the studies[10–12] Thus, we compared the diagnostic accuracy of the AGV image with a combination of various viewing methods, and also with axial images alone.

We found significant coronary artery stenoses were detected on the AGV image with a sensitivity of 98% and specificity of 89%, and with 98% and 93%, respectively, by the conventional methods. Our findings are comparable with those from recent reports of the accuracy of 64-slice CT for the detection of coronary artery stenoses (sensitivity: 93–99%, specificity: 86–97% and NPV 98–99%) analyzed by a combination of conventional methods[2–4,13–15] In the present study, there was only 1 FN finding on the AGV image, which was a very rare lesion located in the just proximal portion of the left circumflex artery where the vessel branches out from the mid-portion of the stent, and the sensitivity of the AGV image was the same as that with the conventional methods. Our results show that the AGV image is a reliable method of identifying significant stenoses.

The accuracy of the AGV image, as with the conventional methods, was significantly higher compared with the axial images alone. Correct diagnosis was more difficult with the axial images than the other viewing methods in the lesions located in the segment running horizontal to the axial section. Diffuse concentric plaque with positive remodeling also has a tendency to be incorrectly viewed as stenotic on axial images, possibly because the reference diameter (vessel diameter in non-diseased artery immediately proximal to the lesion) of these lesions is not measurable on the axial image. For evaluation of these types of lesions, the post-processing image is better suited, although this is a pilot study and thus will require further evaluation.

In a previous study, the sensitivity of the axial image (73.4%) was reported to be superior to virtual angioscopic (49.1%), VR (43.0%), and MPR images (46.8%) from 4-section multidetector CT[8] It seems that axial images are less susceptible to motion artifacts, and the poor results obtained for MPR may have been because strictly orthogonal reformation were obtained only along the centerline of virtual endoscope images and, consequently, segments not captured with VE were also not displayed on the MPRs[16] The 64-detector row CT decreased the frequency of motion artifact, and because the post-processing image can be created in any angle without restrictions, a higher diagnostic accuracy can be expected than with axial images. Another recent study reported high diagnostic accuracy of axial images (sensitivity of 89% and specificity of 89% in assessable arteries and an overall accuracy of 88%) using 16-section multidetector CT[16] This high accuracy may be related to per-artery analysis, not per-segment analysis as in our study, and exclusion of side branches from analysis.

The AGV image is a noninvasive overview of all the coronary arteries and accurately shows the distribution of coronary stenoses in 1 set of images that is understandable by third parties. This would be useful in several situations. First, it would be useful for explaining the severity of disease to the patient. Second, the AGV image can be divided into right and left coronary artery, resembling the images from invasive CAG, which enables viewing the lesions from the same angle as with QCA, and detecting the best angle of the lesion prior to percutaneous coronary intervention would be useful in the discussion of the treatment strategy in conference.

The major drawback of the AGV image is that the specificity for coronary stenosis detection compared with conventional methods was lower, the main cause being overestimation of mild stenoses on QCA as >50% stenoses on the AGV image. Previous studies report that MIP can overestimate the degree of stenosis[17–21] so because the AGV image is a MIP image, the lower specificity is understandable. However, this drawback is considered not to be a problem, because the most important factor for the identification of stenotic lesions is high sensitivity.

It is usually difficult to accurately assess the degree of stenosis of lesions with severe calcification[1–4] In our study, 8 of 24 (33%) lesions with severe calcification were FP on the AGV image, and 7 of 24 (29%) lesions were FP with the conventional methods and on the axial images alone. Further study in a larger number is necessary to clarify the characteristics of each viewing method for the evaluation of lesions with severe calcification.

Study Limitations

First, this was a pilot study and thus the number of subjects was small. Second, QCA was used as the gold standard, but it has its imperfections; stenotic lesions may be missed.

Conclusion

The AGV image shows promise as a reliable post-processing method of identifying coronary artery stenoses. Because the AGV image demonstrates coronary lesions in the 1 image, it would be useful for explaining the severity of disease to the patient, and for discussing the treatment strategy in conference.

References

1. Ropers D, Baum U, Pohle K, Anders K, Ulzheimer S, Ohnesorge B, et al. Detection of coronary artery stenoses with thin-slice multi-detector row spiral computed tomography and multiplanar reconstruction. *Circulation* 2003; **107:** 664–666.
2. Raff GL, Gallagher MJ, O'Neill WW, Goldstein JA. Diagnostic accuracy of noninvasive coronary angiography using 64-slice spiral computed tomography. *J Am Coll Cardiol* 2005; **46:** 552–557.
3. Mollet NR, Cademartiri F, van Mieghem CA, Runza G, McFadden EP, Baks T, et al. High-resolution spiral computed tomography coronary angiography in patients referred for diagnostic conventional coronary angiography. *Circulation* 2005; **112:** 2318–2323.
4. Goldstein JA, Gallagher MJ, O'Neill WW, Ross MA, O'Neil BJ, Raff GL. A randomized controlled trial of multi-slice coronary computed tomography for evaluation of acute chest pain. *J Am Coll Cardiol* 2007; **49:** 863–871.
5. Calhoun PS, Kuszyk BS, Heath DG, Carley JC, Fishman EK. Three-dimensional volume rendering of spiral CT data: Theory and method. *Radiographics* 1999; **19:** 745–764.
6. Feyter PJ, Krestin GP. Image post-processing. *In*: Feyter PJ, Krestin GP, editors. Computed tomography of the coronary arteries. New York: Taylor & Francis; 2005; 27–46.
7. Jinzaki M, Sato K, Tanami Y, Yamada M, Kuribayashi S, Anzai T, et al. Novel method of displaying coronary CT angiography: Angiographic view. *Circ J* 2006; **70:** 1661–1662.
8. Jinzaki M, Yamada M, Sato K, Tanami Y, Anzai T, Sasaki K, et al. Overview image of the lumen and vessel wall in coronary CT angiography: Plaque-loaded angiographic view. *Circ J* 2008; **72:** 671–673.
9. Yamada M, Jinzaki M, Kuribayashi S, Sato K, Tanami Y, Fukumoto K, et al. Novel post-processing image for the visualization of coronary sinus by multidetector-row computed tomography before cardiac resynchronization therapy: Edge-enhanced image. *Circ J* 2008; **72:** 487–488.
10. Pannu HK, Flohr TG, Corl FM, Schoepf UJ. Current concepts in multidetector row CT evaluation of the coronary arteries: Principles, techniques, and anatomy. *Radiographics* 2003; **23:** S111–S125.
11. Ferencik M, Ropers D, Abbara S, Cury RC, Hoffmann U, Nieman K, et al. Diagnostic accuracy of image postprocessing methods for the detection of coronary artery stenoses by using multidetector CT. *Radiology* 2007; **243:** 696–702.
12. Pugliese F, Mollet NR, Runza G, van Mieghem C, Meijboom WB, Malagutti P, et al. Diagnostic accuracy of non-invasive 64-slice CT coronary angiography in patients with stable angina pectoris. *Eur Radiol* 2006; **16:** 575–582.
13. Ropers D, Rixe J, Anders K, Küttner A, Baum U, Bautz W, et al. Usefulness of multidetector row spiral computed tomography with 64-×0.6-mm collimation and 330-ms rotation for the noninvasive detection of significant coronary artery stenoses. *Am J Cardiol* 2006; **97:** 343–348.
14. Vanhoenacker PK, Heijenbrok-Kal MH, Van Heste R, Decramer I, Van Hoe LR, Wijns W, et al. Diagnostic performance of multidetector CT angiography for assessment of coronary artery disease: Meta-analysis. *Radiology* 2007; **244:** 419–428.
15. Achenbach S, Moshage W, Ropers D, Bachmann K. Curved multiplanar reconstructions for the evaluation of contrast-enhanced electron beam CT of the coronary arteries. *Am J Roentgenol* 1998; **170:** 895–899.
16. Vogl TJ, Abolmaali ND, Diebold T, Engelmann K, Ay M, Dogan S, et al. Techniques for the detection of coronary atherosclerosis: Multidetector row CT coronary angiography. *Radiology* 2002; **223:** 212–220.
17. Lu B, Dai RP, Bai H, He S, Jing BL, Jiang SL, et al. Coronary artery stenoses: A phantom study using contrast enhanced three-dimensional electron beam tomography. *Clin Imaging* 2001; **25:** 95–100.
18. Uchino A, Kato A, Kudo S. CT angiography using electron-beam computed tomography (EBCT): A phantom study. *Radiat Med* 1997; **15:** 273–276.
19. Brink JA, Lim JT, Wang G, Heiken JP, Deyoe LA, Vannier MW. Technical optimization of spiral CT for depiction of renal artery stenosis: In vitro analysis. *Radiology* 1995; **194:** 157–163.
20. Dillon EH, van Leeuwen MS, Fernandez MA, Eikelboom BC, Mali WP. CT angiography: Application to the evaluation of carotid artery stenosis. *Radiology* 1993; **189:** 211–219.
21. Rubin GD, Dake MD, Napel S, Jeffrey RB Jr, McDonnell CH, Sommer FG, et al. Spiral CT of renal artery stenosis: Comparison of three-dimensional rendering techniques. *Radiology* 1994; **190:** 181–189.

Atherosclerosis 213 (2010) 166–172

Contents lists available at ScienceDirect

Atherosclerosis

journal homepage: www.elsevier.com/locate/atherosclerosis

Combined presence of aortic valve calcification and mitral annular calcification as a marker of the extent and vulnerable characteristics of coronary artery plaque assessed by 64-multidetector computed tomography

Hiroto Utsunomiya[a], Hideya Yamamoto[a,*], Eiji Kunita[a], Toshiro Kitagawa[a], Norihiko Ohashi[a], Toshiharu Oka[a], Ryo Yamazato[a], Jun Horiguchi[b], Yasuki Kihara[a]

[a] Department of Cardiovascular Medicine, Hiroshima University Graduate School of Biomedical Sciences, 1-2-3 Kasumi, Minami-ku, Hiroshima 734-8551, Japan
[b] Department of Clinical Radiology, Hiroshima University Graduate School of Biomedical Sciences, Hiroshima, Japan

ARTICLE INFO

Article history:
Received 22 June 2010
Received in revised form 13 August 2010
Accepted 18 August 2010
Available online 24 September 2010

Keywords:
Aortic valve calcification
Computed tomography
Mitral annular calcification
Coronary artery plaque
Vulnerability

ABSTRACT

Objective: We examined the association of aortic valve calcification (AVC) and mitral annular calcification (MAC) to coronary atherosclerosis using 64-multidetector computed tomography (MDCT).
Background: Valvular calcification is considered a manifestation of atherosclerosis. The impact of multiple heart valve calcium deposits on the distribution and characteristics of coronary plaque is unknown.
Methods: We evaluated 322 patients referred for 64-MDCT, and assessed valvular calcification and the extent of calcified (CAP), mixed (MCAP), and noncalcified coronary atherosclerotic plaque (NCAP) in accordance with the 17-coronary segments model. We assessed the vulnerable characteristics of coronary plaque with positive remodeling, low-density plaque (CT density ≤38 Hounsfield units), and the presence of adjacent spotty calcification.
Results: In 49 patients with both AVC and MAC, the segment numbers of CAP and MCAP were larger than in those with a lack of valvular calcification and an isolated AVC ($p < 0.001$ for both). Multivariate analyses revealed that a combined presence of AVC and MAC was independently associated with the presence (odds ratio [OR] 9.36, 95% confidence interval [95%CI] 1.55–56.53, $p = 0.015$) and extent (β-estimate 1.86, $p < 0.001$) of overall coronary plaque. When stratified by plaque composition, it was associated with the extent of CAP (β-estimate 1.77, $p < 0.001$) and MCAP (β-estimate 1.04, $p < 0.001$), but not with NCAP. Moreover, it was also related to the presence of coronary plaque with all three vulnerable characteristics (OR 4.87, 95%CI 1.85–12.83, $p = 0.001$).
Conclusion: The combined presence of AVC and MAC is highly associated with the presence, extent, and vulnerable characteristics of coronary plaque identified by 64-MDCT.

1. Introduction

Valvular calcification is generally considered a manifestation of atherosclerosis. Particularly, aortic valve calcification (AVC) and mitral annular calcification (MAC) were reported to be independently associated with both cardiovascular risk factors [1] and coronary artery calcification (CAC) [2,3]. Recent epidemiological studies have also demonstrated that the combined presence of AVC and MAC is independent of and incremental to traditional risk assessment for the prediction of cardiovascular events, and is more strongly associated with cardiovascular mortality than is AVC or MAC alone [4].

Recent advances in contrast-enhanced data acquisition using multidetector computed tomography (MDCT) enabled the detection of calcified coronary atherosclerotic plaque (CAP), mixed coronary atherosclerotic plaque (MCAP), and noncalcified coronary atherosclerotic plaque (NCAP), which was in good agreement with intravascular ultrasound [5,6]. Furthermore, 64-MDCT characterizes coronary plaque in terms of vascular positive remodeling, lipid-rich plaque, and adjacent spotty calcium, which may relate to the fact that vulnerable plaque is prone to rupture with subsequent coronary events [7,8].

Although AVC and MAC are believed to be associated with overall coronary plaque burden using invasive coronary angiography or noncontrast-enhanced CT [2,9], the impact of multiple heart valve

Abbreviations: AVC, aortic valve calcification; CAC, coronary artery calcification; CAD, coronary artery disease; CAP, calcified coronary atherosclerotic plaque; Ccr, creatinine clearance; HU, Hounsfield units; MAC, mitral annular calcification; MCAP, mixed coronary atherosclerotic plaque; MDCT, multidetector computed tomography; NCAP, noncalcified coronary atherosclerotic plaque.

* Corresponding author. Tel.: +81 82 257 5540; fax: +81 82 257 1569.
E-mail address: hideyayama@hiroshima-u.ac.jp (H. Yamamoto).

0021-9150/$ – see front matter © 2010 Elsevier Ireland Ltd. All rights reserved.
doi:10.1016/j.atherosclerosis.2010.08.070

calcium deposits on the distribution and vulnerable characteristics of coronary plaque is unknown. Thus, this study aimed to evaluate the value of the combined presence of AVC and MAC in predicting the extent and vulnerable characteristics of coronary plaque in patients with proven or suspected coronary artery disease (CAD).

2. Methods

2.1. Study population

Between August 2007 and December 2009, we enrolled 578 consecutive patients with proven or suspected CAD who were referred for 64-MDCT for the follow-up or diagnosis of CAD at our institution. Exclusion criteria included prior percutaneous coronary intervention ($n=92$) or coronary artery bypass grafting ($n=90$), irregular heart rhythm including chronic atrial fibrillation ($n=25$), serum creatinine >1.5 mg/dl ($n=15$), prior aortic or mitral valve surgery ($n=8$), acute coronary syndrome ($n=8$), hemodynamic instability ($n=3$), and allergy to iodinated contrast agent ($n=2$). We also excluded 13 patients due to poor image quality ($n=10$) and declined consent ($n=3$). As a result, 322 patients (207 men, 66 ± 11 years) were prospectively enrolled in this study. The study was approved by the Hiroshima University Hospital's ethical committee, and written informed consent was obtained from all patients.

2.2. Covariates and risk factor assessment

Overnight fasting blood samples were collected and the serum total cholesterol, low-density cholesterol, high-density cholesterol, triglyceride, and high-sensitivity C-reactive protein levels were measured. The creatinine clearance (Ccr) was measured by Modification of Diet in Renal Disease study equation. Hypertension was defined as systolic blood pressure >140 mm Hg, diastolic blood pressure >90 mm Hg, or current antihypertensive therapy. Diabetes mellitus was defined as a fasting plasma glucose >126 mg/dl or treatment with a hypoglycemic agent. Hyperlipidemia was defined as a fasting serum total cholesterol of >200 mg/dl or treatment with a lipid-lowering agent. Patients were considered current smokers if they had smoked at least one cigarette per day in the last year.

2.3. MDCT scan protocol

MDCT examinations were performed using a 64-MDCT scanner (LightSpeed VCT, GE Healthcare, Little Chalfont, Buckinghamshire, UK). Before MDCT angiography, a coronary and valve calcium scan was performed with a prospective ECG-triggered at 75% after the R-wave. The precise scan protocol of the retrospective ECG-gated MDCT angiography was previously described [5]. All patients with an initial heart rate ≥60 beats/min were given an oral β-blocker (metoprolol 40 mg) to achieve a target heart rate of 50–60 beats/min. Sublingual nitroglycerin was administrated just before scanning. A body-weight-adjusted volume (0.6–0.7 ml/kg) of iodine contrast (Iopamiron 370, Bayer Healthcare, Berlin, Germany) was administered into the antecubital vein over the course of 10 s, followed by 25 ml of saline solution injected at 5.0 ml/s. The CT reconstructed image data were transferred to an offline workstation (Advantage Workstation Ver. 4.2, GE Healthcare) for post-processing and subsequent image analysis.

2.4. CAC scoring

The total CAC score was calculated based on the Agatston method [10] with dedicated software (Smartscore, version 3.5, GE Healthcare).

2.5. Coronary plaque evaluation

All coronary segments >2 mm in diameter were assessed using thin-slice maximal intensity projections, multiplanar reconstructions, and cross-sectional images rendered perpendicular to the vessel center line of each coronary segment (0.75 mm thickness). The presence and extent of CAP, MCAP, and NCAP were determined for each subject and evaluated in accordance with the modified American Heart Association classification with 17-coronary segments [11].

CAP was defined as any structure with a CT density ≥130 HU that could be visualized separately from the contrast-enhanced coronary lumen, and that could be assigned to the coronary artery wall. MCAP was defined as the presence of CAP and NCAP, either because the calcium was embedded within noncalcified plaque or because they were adjacent to each other within a coronary segment. NCAP was defined as any clearly discernible structure >1 mm^2 that could be assigned to the coronary artery wall in at least two independent image planes, and that had a CT density <130 HU but greater than the surrounding pericardial tissue [12].

We then determined the minimum CT density, vascular remodeling index, and adjacent calcium morphology as previously described [5]. Briefly, the minimum CT density was decided as each plaque density by setting at least five regions of interest (each region area = 1 mm^2) in each plaque area, and low-density plaque was defined as lesions with a CT density ≤38 HU. Following measurement of the cross-sectional vessel areas at each plaque site and proximal reference site of the same coronary artery, we calculated the vascular remodeling index. Positive remodeling was defined as a remodeling index >1.05. The presence and morphology of calcium deposits in or adjacent to each plaque site were determined. Spotty calcium was defined as calcium burden length <3/2 of vessel diameter and width <2/3 of vessel diameter.

2.6. Valvular calcification assessment

The presence of AVC and MAC were qualitatively assessed from both noncontrast and multi-projection images reconstructed from contrast CT datasets. AVC was defined as a calcification lesion just inferior to the origin of the coronary arteries and located at the aortic leaflets, including the valvular point of attachment [3]. MAC was located at the junction between the left atrium and ventricle.

For the subgroup of patients with AVC or MAC, valvular calcification scores were measured with the same software used in CAC scoring. As in prior studies, calcification of the aortic wall immediately connected to calcification of the aortic valve cusps was included in the AVC [2].

2.7. Statistical analysis

Continuous data were presented as mean ± SD or median (interquartile range). Categorical variables were presented as numbers and percentages. The Kruskal–Wallis test or ANOVA was used for group comparisons of continuous variables, and post hoc testing was performed using the Tukey's test or the Steel–Dwass method for variables with and without normal distribution, respectively. Group comparisons of binary variables were performed using Fisher exact or χ^2 test. Multivariate analyses included valvular calcification and were adjusted for potential confounders based on previous reports: age, gender, Ccr, and the traditional risk factors of body mass index, hypertension, diabetes mellitus, hyperlipidemia, current smoking, and family history of premature CAD. Spearman's correlation coefficient was calculated to evaluate the association between the severity of valvular calcification and the extent of coronary atherosclerosis, where log-transformed AVC, MAC, and CAC scores were used. A probability value of $p<0.05$ was considered

significant. All statistical analysis was performed using SPSS 13.0 (SPSS Inc, Chicago, IL).

3. Results

3.1. Patient characteristics

There were 201 subjects (62%) with AVC and 53 (17%) with MAC. Of 17 coronary artery segments, there was an average of 4.2 ± 3.4 segments with any plaque, 3.5 ± 3.3 with CAP, 1.3 ± 1.7 with MCAP, and 0.8 ± 1.2 with NCAP. Of 201 subjects with coronary plaque burden, 84 (26%) had coronary plaque with all three vulnerable characteristics (vascular positive remodeling, low CT density, and adjacent spotty calcification).

Clinical characteristics and CT findings stratified by the presence of valvular calcification are presented in Table 1. The population of isolated MAC was small ($n = 4$); therefore, we excluded this subgroup. Compared with patients with no valvular calcification, those with isolated AVC and those with the combined presence of AVC and MAC were older and had a higher prevalence of hypertension, diabetes mellitus, and hyperlipidemia. There were no significant differences among the three groups in serum lipid and C-reactive protein levels.

3.2. Valvular calcification and overall coronary plaque burden

In a univariate analyses, patients with the combined presence of AVC and MAC had an 11-fold increase odds of having any coronary plaque (odds ratio [OR] 11.16, 95% confidence interval [95%CI] 2.58–48.39, $p = 0.001$) and greater extent of overall coronary plaque burden (β-estimate 2.34, $p < 0.001$) as compared to those with a lack of valvular calcification. After adjustment for age, gender, Ccr, and traditional risk factors, the combined presence of AVC and MAC remained an independent predictor for the presence (OR 9.36, 95%CI 1.55–56.53, $p = 0.015$) and extent (β-estimate 1.86, $p < 0.001$) of coronary plaque, as well as male gender, hypertension, and diabetes mellitus.

3.3. Valvular calcification and the prevalence and distribution of CAP, MCAP, and NCAP

Fig. 1 shows a representative case with the combined presence of AVC and MAC presenting MCAP with vulnerable characteristics. The prevalence and distribution of CAP and MCAP escalated in proportion with the presence of valvular calcification (all $p < 0.001$), whereas the prevalence of NCAP showed no significant difference among the three groups (Table 1). Fig. 2A shows the multivariate adjusted OR for the presence of CAP, MCAP, and NCAP across categories of valvular calcification.

Table 2 summarizes the associations of the combined presence of AVC and MAC to the presence and extent of CAP, MCAP, and NCAP. Multivariate analysis showed that the combined presence of AVC and MAC remained an independent predictor for the presence and extent of CAP (OR 6.21, 95%CI 1.67–23.05, $p = 0.006$; β-estimate 1.77, $p < 0.001$) and MCAP (OR 5.35, 95%CI 1.94–14.73, $p = 0.001$; β-estimate 1.04, $p < 0.001$), as well as male gender and hypertension. Meanwhile, no significant relationship was noted between valvular calcification and NCAP in either univariate or multivariate models.

Table 1
Clinical characteristics and CT findings stratified by the presence of valvular calcification.

Characteristics	None ($N = 118$)	Isolated AVC ($N = 151$)	Combined presence of AVC and MAC ($N = 49$)	p
Clinical data				
Age (years)	59 ± 10	69 ± 9*	73 ± 7*,†	<0.001
Male, n (%)	69 (59)	93 (63)	38 (78)	0.067
Body mass index (kg/m^2)	25 ± 7	24 ± 3	24 ± 4	0.457
Ccr (ml/min)	71 ± 14	67 ± 15	63 ± 15*	0.011
Hypertension, n (%)	60 (51)	116 (77)*	39 (80)*	<0.001
Diabetes mellitus, n (%)	43 (36)	77 (51)*	32 (65)*,†	0.002
Hyperlipidemia, n (%)	48 (41)	88 (58)*	26 (53)*	0.016
Current smoker, n (%)	48 (41)	51 (34)	11 (22)	0.075
Family history of CAD, n (%)	13 (11)	20 (13)	9 (18)	0.442
Total cholesterol (mg/dl)	205 ± 45	202 ± 36	194 ± 34	0.252
Triglycerides (mg/dl)	130 (91–191)	124 (92–173)	119 (87–178)	0.801
HDL cholesterol (mg/dl)	60 ± 19	59 ± 18	62 ± 21	0.565
LDL cholesterol (mg/dl)	123 ± 36	119 ± 29	112 ± 27	0.102
High-sensitivity CRP (mg/l)	0.5 (0.3–1.0)	0.6 (0.3–1.4)	0.8 (0.3–2.1)	0.260
Lipid-lowering agents, n (%)	21 (18)	47 (31)*	18 (37)*	0.013
CT findings				
CAC score	6 (0–51)	152 (27–476)*	288 (102–1020)*,†	<0.001
Prevalence of CAP, n (%)	62 (53)	131 (87)*	47 (96)*,†	<0.001
Prevalence of MCAP, n (%)	44 (37)	93 (62)*	39 (80)*,†	<0.001
Prevalence of NCAP, n (%)	44 (37)	78 (52)	25 (51)	0.059
Extent of CAP (segments)	1.7 ± 2.4	3.3 ± 2.3*	5.4 ± 3.4*,†	<0.001
Extent of MCAP (segments)	0.6 ± 0.9	1.6 ± 1.8*	2.3 ± 2.0*,†	<0.001
Extent of NCAP (segments)	0.6 ± 0.9	1.0 ± 1.4*	0.9 ± 1.4	0.013
Positive remodeling, n (%)	36 (31)	96 (64)*	37 (76)*,†	<0.001
Low CT density, n (%)	45 (38)	82 (54)*	31 (63)*	<0.001
Spotty calcification, n (%)	37 (31)	74 (49)*	29 (59)*	0.001
All three vulnerable characteristics, n (%)	19 (16)	44 (29)*	21 (43)*,†	0.001

Values are mean ± SD, number (percentage), or median (interquartile range). AVC = aortic valve calcification; CAC = coronary artery calcification; CAD = coronary artery disease; CAP = calcified coronary atherosclerotic plaque; Ccr = creatinine clearance; CRP = C-reactive protein; CT = computed tomography; HDL = high-density lipoprotein; LDL = low-density lipoprotein; MAC = mitral annular calcification; MCAP = mixed coronary atherosclerotic plaque; NCAP = noncalcified coronary atherosclerotic plaque.

* $p < 0.05$ vs. none.

† $p < 0.05$ vs. isolated AVC.

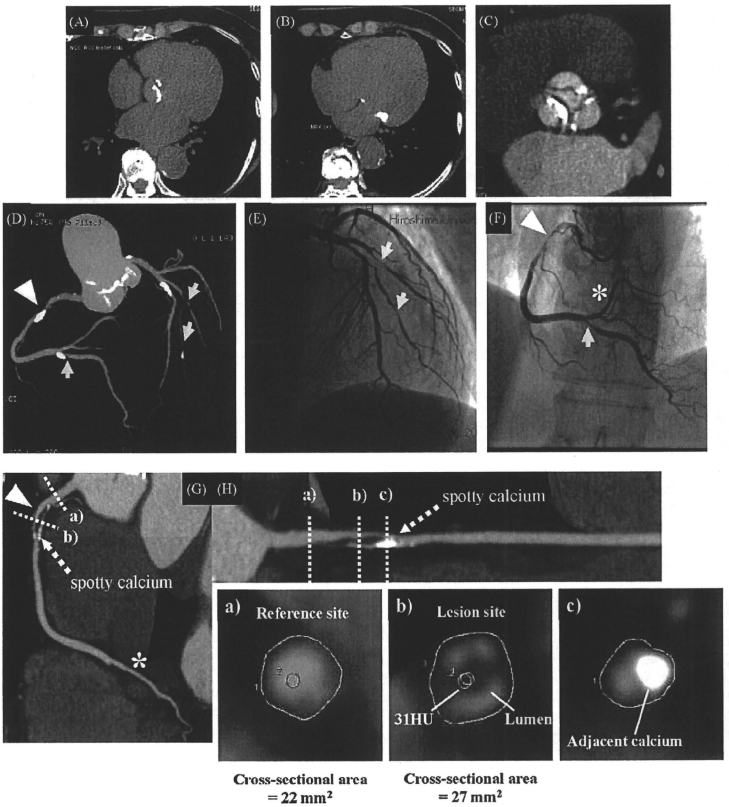

Fig. 1. A representative case with the combined presence of aortic valve calcification (AVC) (panel A) and mitral annular calcification (MAC) (panel B) presenting mixed coronary atherosclerotic plaque (MCAP) with vulnerable characteristics The double oblique transversal image shows calcified lesions at all leaflets (panel C). The maximum intensity projection image and invasive coronary angiography shows a severe stenosis of the proximal portion of the right coronary artery (arrowhead) and multiple obstructive lesions (panels D–F, yellow arrow). The multiplanar reconstruction image of the right coronary artery shows an obstructive MCAP with positive vascular remodeling and adjacent spotty calcium (panels G and H). The remodeling index is 1.23, calculated from the cross-sectional images of the reference site (a) and the lesion site (b). The minimum CT density of the lesion site is 31 HU. Adjacent spotty calcium can be observed in the cross-sectional image (c). (For interpretation of the references to colour in this figure legend, the reader is referred to the web version of the article.)

Table 2
Univariate and multivariate models for the associations of the combined presence of AVC and MAC to the presence and extent of CAP, MCAP, and NCAP.

	Presence		Extent	
	Odds ratio (95%CI)	*p*	*β*-estimate (95%CI)	*p*
CAP				
Univariate model	10.16 (3.44–30.06)	<0.001	2.27 (1.29–3.25)	<0.001
Multivariate model[a]	6.21 (1.67–23.05)	0.006	1.77 (0.83–2.72)	<0.001
MCAP				
Univariate model	6.56 (2.98–14.43)	<0.001	1.09 (0.60–1.59)	<0.001
Multivariate model[a]	5.35 (1.94–14.73)	0.001	1.04 (0.56–1.53)	<0.001
NCAP				
Univariate model	1.75 (0.89–3.43)	0.10	0.11 (−0.27–0.49)	0.56
Multivariate model[a]	1.45 (0.64–3.28)	0.37	−0.02 (−0.42–0.40)	0.97

CI = confidence interval. Other abbreviations as Table 1.

[a] Adjusted for age, gender, Ccr, and traditional risk factors including body mass index, hypertension, diabetes mellitus, hyperlipidemia, current smoking, and family history of coronary artery disease.

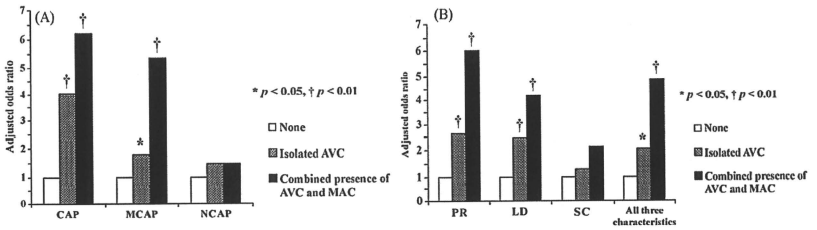

Fig. 2. Open bars represent no valvular calcification; hashed bars, isolated aortic valve calcification (AVC); solid bars, combined presence of AVC and mitral annular calcification (MAC). (A) Multivariate adjusted odds ratio for the presence of calcified coronary atherosclerotic plaque (CAP), mixed coronary atherosclerotic plaque (MCAP), and noncalcified coronary atherosclerotic plaque (NCAP) across categories of valvular calcification. (B) Multivariate adjusted odds ratio for the presence of coronary plaque with vulnerable characteristics (positive vascular remodeling [PR], low CT density [LD], adjacent spotty calcification [SC], and all three characteristics) across categories of valvular calcification.

3.4. Valvular calcification and coronary plaque with vulnerable characteristics

Patients with the combined presence of AVC and MAC had a higher frequency of coronary plaque with all three vulnerable characteristics than those with either no valvular calcification or isolated AVC (43% vs. 16% vs. 29%, respectively; $p = 0.001$). Fig. 2B depicts the multivariate adjusted OR for the presence of coronary plaque with vulnerable characteristics across categories of valvular calcification. Multivariate analysis showed that the combined presence of AVC and MAC remained an independent predictor for the presence of coronary plaque with all three vulnerable characteristics (OR 4.87, 95%CI 1.85–12.83, $p = 0.001$).

3.5. Valvular calcification score and the extent of coronary plaque

In a subgroup of patients with AVC ($n = 201$, 62%), the median AVC score was 77 (interquartile range 27–214). The AVC score correlated with the extent of coronary plaque, but its composition varied (Table 3). Multivariate analysis revealed that the log-transformed AVC score was not associated with the extent of CAP ($p = 0.07$), MCAP ($p = 0.19$), or NCAP ($p = 0.92$).

In a subgroup of patients with MAC ($n = 53$, 17%), the median MAC score was 82 (interquartile range 27–190). The MAC score did not correlate with the extent of coronary plaque ($p = 0.72$).

4. Discussion

Our study demonstrates the relationship between valvular calcification and the presence of coronary plaque with positive vascular remodeling, low CT density, and adjacent spotty calcium, which may represent vulnerable characteristics as previously reported [7,8]. These data suggest the presence of a common atherosclerotic pathway for development of valvular calcification and coronary plaque, and emphasize the importance of the combined presence of AVC and MAC as a marker of subclinical CAD.

Table 3
Age- and gender-adjusted Spearman's correlation coefficients in patients with AVC ($n = 201$).

	Log(AVC+1)	Log(CAC+1)	CAP	MCAP	NCAP
Log(AVC+1)	–				
Log(CAC+1)	0.28*	–			
CAP	0.29*	0.88*	–		
MCAP	0.22†	0.53*	0.63*	–	
NCAP	−0.002	−0.12	−0.16‡	0.03	–

Abbreviations as Table 1.
* $p < 0.001$ for all correlations.
† $p < 0.01$ for all correlations.
‡ $p < 0.05$ for all correlations.

4.1. Association between valvular calcification and coronary plaque burden

We demonstrate that valvular calcification is a marker of higher prevalence and severity of coronary plaque, particularly CAP and MCAP, independent of age and gender. The prevalence of AVC and MAC definitely increases with age [1], but is strongly related to traditional cardiovascular risk factors, including diabetes mellitus, hypertension [3], and hyperlipidemia [2]. Thus far, several studies have demonstrated a strong association of AVC or MAC with coronary microvascular endothelial dysfunction [13] and CAC, a marker of overall coronary atherosclerotic plaque burden [2,3]. Based on these data, it is believed that valvular calcification is a manifestation of atherosclerosis and is associated with CAD. However, paucity data exists regarding a direct association between the combined presence of AVC and MAC and the distribution of noncalcified plaque. Indeed, there is strong evidence that the severity of CAC is independent of and incremental to traditional risk factors for all-cause mortality and cardiovascular events [14]; whereas in a recent study, the number of segments with MCAP was an independent predictor of acute cardiac events [15]. Thus, our findings link the combined presence of AVC and MAC to the excess MCAP burden that leads to acute coronary events, and may assure early detection of MCAP for more accurate assessment of cardiovascular risk.

In this study, the combined presence of AVC and MAC was significantly associated with the presence and extent of MCAP, but not NCAP. Interestingly, Bamberg et al. recently demonstrated that the association between MCAP and NCAP was not constant but changed with age, indicating that the former is prominent in the early stages of atherosclerosis, whereas the latter develops during the chronic phase [16]. Therefore, our results suggest that the presence of multiple calcium deposits in heart valves could be a surrogate marker for the advanced stages of atherosclerosis. This observation is in agreement with a recent study that shows a significant relationship between AVC and the extent of coronary artery plaque [17].

4.2. Association between valvular calcification and coronary plaque vulnerability

Our study provides novel information on the age-independent association between valvular calcification and the vulnerable characteristics of coronary plaque. Several cohort studies have shown that patients with AVC [18] or MAC [19] had a higher risk of all-cause mortality and cardiovascular events, especially acute

coronary syndrome. In a recent report, the associations of AVC and MAC with cardiovascular mortality were strongest in patients with the combined presence of AVC and MAC [4]. Furthermore, an association between thoracic aortic calcification with total mortality was found in a prospective study with great number of subjects [20]. These data support the hypothesis that multiple calcium deposits in heart valves and thoracic aorta are a form of more advanced atherosclerosis with a high frequency of unstable coronary plaque, explaining its association with an increased risk of cardiovascular events.

A recent MDCT study demonstrated that noncalcified plaque is more strongly associated with the pathogenesis of acute coronary syndrome compared with CAP [7]. In addition, positive vascular remodeling, low CT density, and adjacent spotty calcium represent the coronary plaque vulnerability detected by 64-MDCT [8]. Considering our findings, we suggest that the combined presence of AVC and MAC may be used to improve risk stratification in clinical practice. Future prospective studies should evaluate whether the combined presence of AVC and MAC identifies patients at high risk for ischemic events, and whether medical treatment prevents these events.

4.3. Amounts of valvular calcification and subclinical coronary artery atherosclerosis

In this study, the severity of AVC was not independently associated with the extent of coronary plaque. In clinical practice, severe aortic stenosis caused by massive AVC with no obstructive CAD is often seen. These cases would be inapprehensible with a solely atherosclerotic mechanism of AVC progression. Recent noncontrast-enhanced CT studies have shown the two different phases of AVC progression: the early phase, when AVC appears *de novo* with progressive atherosclerosis, and the secondary phase, when established AVC progresses independently of cardiovascular risk factors and grows faster with calcification load [2]. Regarding MAC, echocardiographic severity has been directly related to the increased risk of cardiovascular events [19], whereas MAC severity was not correlated with the extent of coronary plaque in this study. Overall, our findings indicate that the combined presence of AVC and MAC is a marker of the presence and extent of coronary plaque, but massive valvular calcification is not a marker for extensive coronary plaque.

4.4. Limitations

This study was limited by a relatively small sample size. Our results cannot be generated because this is an observational and cross-sectional study. Thus, larger observational studies are necessary to confirm our findings. The study population was comprised of patients with proven or suspected CAD. A high prevalence of traditional risk factors and AVC were observed in this study. Thus, our results do not apply to patients with a lower probability of CAD. Furthermore, an additional mechanism related to renal insufficiency and osteoporosis may be responsible for the development of MAC. Because there were very few patients with isolated MAC in this study, the exact association between MAC and coronary plaque is not clear. However, the combined presence of AVC and MAC was shown to be incremental to isolated AVC in the prediction of coronary plaque with vulnerable characteristics.

Finally, cardiac MDCT examination should not be used for the sole purpose of AVC and MAC assessment due to its high radiation exposure. However, in this study, we performed 64-MDCT for the primary purpose of CAD assessment. The images obtained enabled evaluation of the association between valvular calcification and the extent and vulnerable characteristics of coronary atherosclerotic plaque.

5. Conclusions

Our study provides the first insight into the impact of the combined presence of AVC and MAC on the presence, extent, and vulnerable characteristics of coronary plaque in patients with proven or suspected CAD. The presence of multiple calcium deposits in heart valves is a useful marker for advanced coronary atherosclerosis, and is likely to help identify appropriate patients for aggressive medical therapy to inhibit the atherosclerosis process.

Conflict of interest

The authors declare no conflicts of interest.

Acknowledgements

This study was supported by grants from the Ministry of Health, Labour and Welfare, Japan (Tokyo, Japan). The authors are grateful to Masao Kiguchi, RT and Chikako Fujioka, RT for their technical assistance.

References

[1] Stewart BF, Siscovick D, Lind BK, et al. Clinical factors associated with calcific aortic valve disease. Cardiovascular Health Study. J Am Coll Cardiol 1997;29:630–4.
[2] Messika-Zeitoun D, Bielak LF, Peyser PA, et al. Aortic valve calcification: determinants and progression in the population. Arterioscler Thromb Vasc Biol 2007;27:642–8.
[3] Allison MA, Cheung P, Criqui MH, Langer RD, Wright CM. Mitral and aortic annular calcification are highly associated with systemic calcified atherosclerosis. Circulation 2006;113:861–6.
[4] Volzke H, Haring R, Lorbeer R, et al. Heart valve sclerosis predicts all-cause and cardiovascular mortality. Atherosclerosis 2010;209:606–10.
[5] Kitagawa T, Yamamoto H, Ohhashi N, et al. Comprehensive evaluation of noncalcified coronary plaque characteristics detected using 64-slice computed tomography in patients with proven or suspected coronary artery disease. Am Heart J 2007;154:1191–8.
[6] Leber AW, Knez A, von Ziegler F, et al. Quantification of obstructive and nonobstructive coronary lesions by 64-slice computed tomography: a comparative study with quantitative coronary angiography and intravascular ultrasound. J Am Coll Cardiol 2005;46:147–54.
[7] Motoyama S, Sarai M, Harigaya H, et al. Computed tomographic angiography characteristics of atherosclerotic plaques subsequently resulting in acute coronary syndrome. J Am Coll Cardiol 2009;54:49–57.
[8] Kitagawa T, Yamamoto H, Horiguchi J, et al. Characterization of noncalcified coronary plaques and identification of culprit lesions in patients with acute coronary syndrome by 64-slice computed tomography. JACC Cardiovasc Imaging 2009;2:153–60.
[9] Yamamoto H, Shavelle D, Takasu J, et al. Valvular and thoracic aortic calcium as a marker of the extent and severity of angiographic coronary artery disease. Am Heart J 2003;146:153–9.
[10] Agatston AS, Janowitz WR, Hildner FJ, Zusmer NR, Viamonte Jr M, Detrano R. Quantification of coronary artery calcium using ultrafast computed tomography. J Am Coll Cardiol 1990;15:827–32.
[11] Raff GL, Abidov A, Achenbach S, et al. SCCT guidelines for the interpretation and reporting of coronary computed tomographic angiography. J Cardiovasc Comput Tomogr 2009;3:122–36.
[12] Hoffmann U, Bamberg F, Chae CU, et al. Coronary computed tomography angiography for early triage of patients with acute chest pain: the ROMICAT (Rule Out Myocardial Infarction using Computer Assisted Tomography) trial. J Am Coll Cardiol 2009;53:1642–50.
[13] Bozbas H, Pirat B, Yildirir A, et al. Mitral annular calcification associated with impaired coronary microvascular function. Atherosclerosis 2008;198:115–21.
[14] Budoff MJ, Shaw LJ, Liu ST, et al. Long-term prognosis associated with coronary calcification: observations from a registry of 25,253 patients. J Am Coll Cardiol 2007;49:1860–70.
[15] Pundziute G, Schuijf JD, Jukema JW, et al. Prognostic value of multislice computed tomography coronary angiography in patients with known or suspected coronary artery disease. J Am Coll Cardiol 2007;49:62–70.
[16] Bamberg F, Dannemann N, Shapiro MD, et al. Association between cardiovascular risk profiles and the presence and extent of different types of coronary atherosclerotic plaque as detected by multidetector computed tomography. Arterioscler Thromb Vasc Biol 2008;28:568–74.
[17] Mahabadi AA, Bamberg F, Toepker M, et al. Association of aortic valve calcification to the presence, extent, and composition of coronary artery